Available Online at http://www.journalajst.com

ASIAN JOURNAL OF SCIENCE AND TECHNOLOGY

ISSN: 0976-3376

Asian Journal of Science and Technology
Vol. 15, Issue, 01, pp. 12856-12860, January, 2024

RESEARCH ARTICLE

FIDELITY OF BELL STATE MEASUREMENTS USING IBM 7-QUBIT OPEN ACCESS QUANTUM PROCESSOR ibmq_nairobi

B. P. Govindaraja*[1], H. Talath[2], B. G. Divyamani[3], Akshata H Shenoy[4], A. R. Usha Devi[2] and Sudha[1]

[1]Department of Physics, Kuvempu University, Shankaraghatta-577451, India
[2]Department of Physics, Bangalore University, Jnanabharathi, Bengaluru-560056, India
[3]Tunga Mahavidyalaya, Thirthahalli 577432, India
[4]International Centre for Theory of Quantum Technologies, University of Gdánsk, Gdánsk, Poland

ARTICLE INFO

Article History:
Received 10th October, 2023
Received in revised form
18th November, 2023
Accepted 09th December, 2023
Published online 30th January, 2024

Keywords:
Bell states, Tomography, Fidelity.

ABSTRACT

Entanglement is a key resource in the field of quantum computation and quantum technologies. One has to deal with *measurement error-mitigation* in the present day Noisy Intermediate-scale Quantum (NISQ) processors so as to witness advantages offered by entanglement. In this paper we implement Bell state measurements in IBM open access 7-qubit quantum processor *ibmq_nairobi* and mitigate errors incurred. We evaluate fidelities of all *four* Bell states (theoretical) with the ones retrieved experimentally before and after measurement error-mitigation. Our results reveal a clear enhancement in *quantum fidelity* after error-mitigation methods are employed.

Citation: ***B. P. Govindaraja, Talath Humera, B. G. Divyamani, Akshata H Shenoy, A. R. Usha Devi and Sudha.*** **2024.** "Fidelity of bell state measurements using ibm 7-qubit open access quantum processor Ibmq_Nairobi", *Asian Journal of Science and Technology*, 15, (01), 12856-12860.

INTRODUCTION

Quantum computers are sought after in quantum technology as they exhibit the potential to outperform their classical counterparts (J. Preskill, 2018). However, the aim to build large-scale quantum processors with the ability to execute real-time computations faces many hurdles. Noise is one of the central obstacles that limits the performance of quantum computers of the Noisy Intermediate-scale Quantum (NISQ) era (J. Preskill, 2018, A. Montanaro, 2016). While developing fault-tolerant processors protected by quantum error-correction serves as an ideal approach to minimize noise, it requires each of the logical qubits to be encoded into several physical qubits. In other words, an overhead cost on qubits for encoding the logical information is vital with the approach based on quantum error-correction. One finds that the noise present in the NISQ quantum processors is too high for the execution of efficient error-correction codes(D. Qin, *et. al,*2022).Alternate method of suppressing quantum noise is to *mitigate* errors than *correcting* it (D. Qin, *et. al,* 2022;A. W. R. Smith, *et. al,* 2021). One has to ascertain how close are the solutions obtained after error-mitigation to the ideal ones. Quantum error-mitigation helps in establishing the quantum advantage for certain applications on NISQ devices. Dedicated efforts have thus been put in towards proof-of-principle tests in various available quantum processors. Cloud quantum computing based on IBM's quantum network (IBM, 2023) has made it possible for global users around the world to explore quantum information processing without their own hardware devices.

In the present work, wefocus on implementing Bell measurements and mitigating measurement errors. We employ theIBM open access 7-qubit quantum processor *ibmq_nairobi* for this purpose. We carry out 5 trials of Bell state measurements with 20,000 shots each onthe qubits q0, q1 of *ibmq_nairobi* processor. We evaluate fidelities of all *four* Bell states (theoretical) with the experimentally reconstructed ones before and after error-mitigation.

Organization of our paper is as follows: In Section 2 we give a basic description of one and two qubit gates& quantum circuits for the construction of all four Bell states. Section 3 gives a brief overview of the architecture of the 7-qubit quantum processor *ibmq_nairobi*. Probabilities of measurement outcomes in 5 different trials (with 20,000 shots/trial) of the Bell state measurement on *all* 4 input Bell states are subjected toerror-mitigation. This is followed by the reconstruction of Bell state density matrices. In Section 4, we evaluate quantum fidelity of Bell states (theoretical)with the experimentally reconstructed ones before and after error-mitigation. Section 5 contains a short summary of our results.

Qubit Gates and Measurements*:* A chosen set of one qubit gates i.e., Hadamard & X, Y, Z (which are 2×2 Pauli matrices), Rotation gates and two qubit Controlled NOT or CNOT gatehas been employed in quantum computation task. Any arbitrary unitary transformation on n-qubit state can be constructed using these single and two-qubit gates (A. Barenco, *et.al,* 1993). In Table 1 we illustrate the symbols and mathematical representation of qubits, gates and measurements.

Circuit symbol & Matrix Representaion
Qubit: $\|0\rangle = \begin{pmatrix}0\\1\end{pmatrix}$ $\|1\rangle = \begin{pmatrix}1\\0\end{pmatrix}$
Hadamard Gate: $H = \frac{1}{\sqrt{2}}\begin{bmatrix}1 & 1\\1 & -1\end{bmatrix}$
Rotation Gate: $R_x(\theta) = \begin{pmatrix}\cos\frac{\theta}{2} & -i\sin\frac{\theta}{2}\\ -i\sin\frac{\theta}{2} & \cos\frac{\theta}{2}\end{pmatrix}$
CNOT Gate $\text{CNOT} = \begin{bmatrix}1&0&0&0\\0&1&0&0\\0&0&0&1\\0&0&1&0\end{bmatrix}$
Z measurements with outcomes 0, 1 $\prod_1 = \begin{pmatrix}0&0\\0&1\end{pmatrix}$

Table 2. Quantum tomographic scheme for 2-qubit system

Tomographic operations	Experimental probabilities of z measurements on both the qubits with outcomes $i,j = 0,1$	Elements of ρ
$I \otimes I$	$\vec{P}_{zz} = \{P_{zz}(i,j) = \text{Tr}(\rho\ \Pi_i \otimes \Pi_j)\}$	$\rho_{11}, \rho_{22}, \rho_{33}, \rho_{44}$
$H \otimes I$	$\vec{P}_{Hzz} = \{P_{Hzz}(i,j) = \text{Tr}(\rho\ H\ \Pi_i\ H \otimes \Pi_j)\}$	$\text{Re}\rho_{13}, \text{Re}\rho_{24}$
$I \otimes R_X(\pi/2)$	$\vec{P}_{zRz} = \{P_{zRz}(i,j) = \text{Tr}(\rho\ \Pi_i \otimes R_X(\pi/2)\ \Pi_j R_X{}^{\dagger}(\pi/2))\}$	$\text{Im}\rho_{12}, \text{Im}\rho_{34}$
$I \otimes H$	$\vec{P}_{zHz} = \{P_{zHz}(i,j) = \text{Tr}(\rho\ \Pi_i \otimes H\ \Pi_j H\}$	$\text{Re}\rho_{13}, \text{Re}\rho_{24}$
$R_X(\pi/2) \otimes I$	$\vec{P}_{Rzz} = \{P_{Rzz}(i,j) = \text{Tr}(\rho\ R_X(\pi/2)\ \Pi_i R_X{}^{\dagger}(\pi/2)) \otimes \Pi_j\}$	$\text{Im}\rho_{13}, \text{Im}\rho_{24}$
$(H \otimes I)$ CNOT	$\vec{P}_{CHzz} = \{P_{CHzz}(i,j) = \text{Tr}(\rho\ \text{CNOT}H\ \Pi_i H \otimes \Pi_j\ \text{CNOT}\}$	$\text{Re}\rho_{14}, \text{Re}\rho_{23}$
$(R_X(\pi/2) \otimes)$ CNOT	$\vec{P}_{CRzz} = \{P_{CHzz}(i,j) = \text{Tr}(\rho\ \text{CNOT}R_X\ \Pi_i R_X{}^{\dagger}\ \Pi_i H \otimes \Pi_j\ \text{CNOT}\}$	$\text{Im}\rho_{14}, \text{Im}\rho_{23}$

Density Matrix of 2-qubit system: A 2-qubit system is characterized by a 4×4 density matrix.

$$\rho = \begin{pmatrix}\rho_{00;00} & \rho_{00;01} & \rho_{00;10} & \rho_{00;11}\\ \rho_{01;00} & \rho_{01;01} & \rho_{01;10} & \rho_{01;11}\\ \rho_{10;00} & \rho_{10;01} & \rho_{10;10} & \rho_{10;11}\\ \rho_{11;00} & \rho_{11;01} & \rho_{11;10} & \rho_{11;11}\end{pmatrix} \equiv \begin{pmatrix}\rho_{11} & \rho_{12} & \rho_{13} & \rho_{14}\\ \rho_{21} & \rho_{22} & \rho_{23} & \rho_{24}\\ \rho_{31} & \rho_{32} & \rho_{33} & \rho_{34}\\ \rho_{41} & \rho_{42} & \rho_{43} & \rho_{44}\end{pmatrix}$$

which satisfies the properties (i) Hermiticity: $\rho = \rho^{\dagger}$(ii) Unit trace condition: Tr ρ=1 (iii) Positive semi-definiteness: $\rho \geq 0$. These properties lead to $2^4 - 1 = 15$ real independent parameters governing the 2-qubit density matrix. In order to determine the real independent elements of 2-qubit density matrix, the tomography scheme (S. Dogra *et al.,* 2021, H. Talath *et al.,* 2023) involving a set of 7 measurements has been employed (see Table 2). It is clear from explicit evaluation that

$\vec{P}_{zz}$=$(\rho_{11}, \rho_{22}, \rho_{33}, \rho_{44})^T$, $P_{Hzz}(0,0) - P_{Hzz}(1,0)$= 2 Re$\rho_{13}$,
$P_{Hzz}(0,1) - P_{Hzz}(1,1)$= 2 Re$\rho_{24}$,
$P_{zHz}(0,0) - P_{zHz}(0,1)$=2 Re$\rho_{12}$,$P_{zHz}(1,0) - P_{\boldsymbol{zHz}}(1,1)$=2 Re$\rho_{34}$,
$P_{zRz}(0,0) - P_{zRz}(0,1) = 2\ \text{Im}\rho_{12}$,$P_{zRz}(1,0) - P_{\boldsymbol{zRz}}(1,1)$= 2Im$\rho_{34}$,
$P_{Rzz}(0,0) - P_{Rzz}(1,0) = 2\ \text{Im}\rho_{13}$, $P_{Rzz}(0,1) - P_{\boldsymbol{Rzz}}(1,1)$= 2 Im$\rho_{24}$,
$P_{CHzz}(0,0) - P_{CHzz}(1,0) = 2\ \text{Re}\rho_{14}$, $P_{CHzz}(0,1) - P_{CHzz}(1,1) =$ 2 Reρ_{23},
$P_{CRzz}(0,0) - P_{CRzz}(1,0) = 2\ \text{Im}\rho_{14}$, $P_{CRzz}(0,1) - P_{CRzz}(1,1) =$ 2 Imρ_{23}.

Bell States: Bell states $\{|\Phi_{\pm}\rangle = \frac{|00\rangle \pm |11\rangle}{\sqrt{2}}$, $|\Psi_{\pm}\rangle = \frac{|01\rangle \pm |10\rangle}{\sqrt{2}}\}$ form maximally entangled orthogonal & complete set of basis states of the two-qubit Hilbert space.

Density matrices of Bell states are given by,

$$\rho_{\Phi_{\pm}} = |\Phi_{\pm}\rangle\langle\Phi_{\pm}| = \frac{1}{2}\begin{bmatrix}1 & 0 & 0 & \pm 1\\ 0 & 0 & 0 & 0\\ 0 & 0 & 0 & 0\\ \pm 1 & 0 & 0 & 1\end{bmatrix},$$

$$\rho_{\Psi_{\pm}} = |\Psi_{\pm}\rangle\langle\Psi_{\pm}| = \frac{1}{2}\begin{bmatrix}0 & 0 & 0 & 0\\ 0 & 1 & \pm 1 & 0\\ 0 & \pm 1 & 1 & 0\\ 0 & 0 & 0 & 0\end{bmatrix}$$

Here we consider the set of four Bell states $\{|\Phi_+\rangle, |\Phi_-\rangle, |\Psi_+\rangle, |\Psi_-\rangle\}$ for our tomographic construction. We need not carry out all 7 tomographic operations given in Table 2 in this particular case. Itsuffices to implement the tomographic operation $(H \otimes I)$ CNOT followed by z measurement on both the qubits.The tomographic operation $(H \otimes I)$ CNOT followed by z measurements on the qubits corresponds to complete orthonormal measurements constituted by the Bell state basis:

$$\text{CNOT}(H\ \Pi_0 H \otimes \Pi_0)\text{CNOT} = \frac{1}{2}\begin{pmatrix}1 & 0 & 0 & 1\\ 0 & 0 & 0 & 0\\ 0 & 0 & 0 & 0\\ 1 & 0 & 0 & 1\end{pmatrix} = |\Phi_+\rangle\langle\Phi_+|$$

$$\text{CNOT}\left(H\ \Pi_0 H \otimes \Pi_1\right)\text{CNOT} = \frac{1}{2}\begin{pmatrix}0 & 0 & 0 & 0\\ 0 & 1 & 1 & 0\\ 0 & 1 & 1 & 0\\ 0 & 0 & 0 & 0\end{pmatrix} = |\Psi_+\rangle\langle\Psi_+|$$

$$\text{CNOT}\left(H\ \Pi_1 H \otimes \Pi_0\right)\text{CNOT} = \frac{1}{2}\begin{pmatrix}1 & 0 & 0 & -1\\ 0 & 0 & 0 & 0\\ 0 & 0 & 0 & 0\\ -1 & 0 & 0 & 1\end{pmatrix} = |\Phi_-\rangle\langle\Phi_-|$$

$$\text{CNOT}\left(H\,\Pi_1 H \otimes \Pi_1\right)\text{CNOT} = \frac{1}{2}\begin{pmatrix} 0 & 0 & 0 & 0 \\ 0 & 1 & -1 & 0 \\ 0 & -1 & 1 & 0 \\ 0 & 0 & 0 & 0 \end{pmatrix} = |\Psi_-\rangle\langle\Psi_-|$$

and is useful for Bell state tomography. We employ the above measurement scheme to reconstruct Bell states using the *ibmq_nairobi* quantum processor and apply error-mitigation methods.

Details of the Experiment and measurement error-mitigation: We had limited open access (10 minutes per month) to IBM quantum chips. We implemented our experimental scheme using the *zeroth* and *first* qubits q_0, q_1 of IBM 7-qubit processor *ibmq_nairobi*. Architecture and characteristics of qubits q_0, q_1 of *ibmq_nairobi*is given in Figure 1).

We created the Bell states $|\Phi_\pm\rangle = \frac{|00\rangle \pm |11\rangle}{\sqrt{2}}$, $|\Psi_\pm\rangle = \frac{|01\rangle \pm |10\rangle}{\sqrt{2}}$ (see Figure. 2 for the quantum circuits creating Bell states) and carried out 5 trials with 20,000 shots per trial of the $(H \otimes I)$ CNOT tomography operations (see Figure 3 for the quantum circuits corresponding to the tomography operations) on qubits q_0, q_1 of *ibmq_nairobi* quantum processor. With input Bell states we implemented $(H \otimes I)$ CNOT tomographic operation (See Figure 3) and carried out Z measurements on qubits q_0, q_1. We carried out five different trials, with 20,000 shots per trial on all four Bell states. Counts recorded in one of the trials for all four Bell states are shown in Figure 4.

Architecture of 7-qubit quantum processor *ibmq_nairobi*

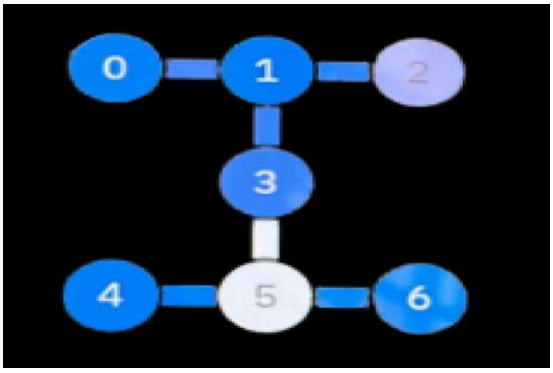

Readout assignment error

CNOT error

Calibration characteristics of qubits q0, q1

Qubit	T1 (μs)	T2 (μs)	Error P(0|1)	Error P(1|0)	CNOT error
0	98.75	32.37	0.0320	0.0132	0.00918
1	126.96	88.59	0.0286	0.0114	

T1: Energy relaxation time, T2: Dephasing time

Figure1. Architecture and experimental parameters for the qubits q_0, q_1 of the 7-qubit superconducting quantum processor *ibmq_nairobi* (Credit-IBM)

Quantum error-mitigation: Quantum error-mitigation approach (D. Qin, *et. al,* 2022; A. W. R. Smith, *et. al,* 2021; S. Dogra *et. al,* 2021) is useful to reduce the damage caused by noisy qubits. We consider the experimentally extracted probability vector $\vec{p}_\alpha = \text{Tr}\,(M_\alpha\,\rho\,{M_\alpha}^\dagger)$ associated with the outcome $\alpha = 0,1$ of a specific measurement operator $M_\alpha$on a qubit state, characterized by the density matrix ρ. One may wrongly obtain the outcome 1 when the qubit is in fact prepared in the state $|0\rangle$. Similarly, it is possible to register the result 0 for the input qubit state $|1\rangle$in a noisy measurement. Corrected probability vector ${\vec{p}_{\text{corr}}}^{(i)} = {F_i}^{-1}\,\vec{p}^{(i)}$ is obtained with the help of the 2×2calibration matrix.

$$F_i = \begin{pmatrix} f_0^{(i)} & 1-f_1^{(i)} \\ 1-f_0^{(i)} & f_1^{(i)} \end{pmatrix},$$

where $f_{0(1)}^{(i)}$= probability of correctly finding 0 (1) when the i^{th}qubit (which is subjected to measurement process) is in the state 0 (1) and $1 - f_{0(1)}^{(i)}$= probability of wrongly obtaining 0 (1) when the i^{th} qubit is in state 0 (1). Corrected two-qubit probability vector is constructed by using ${\vec{p}_{\text{corr}}}^{(q0,q1)} = F_{q0,q1}^{-1}\,\vec{p}^{(q0,q1)}$ where the two-qubit calibration matrix corresponding to measurements on two of the qubits q_0, q_1, is given by the 4×4 matrix $F_{q0,q1} = F_{q0} \otimes F_{q1}$.We found the 2×2 calibration matrices for qubits q_0, q_1 of *ibmq_nairobi* (based on 20,000 runs each with 0 and 1 as inputs) to be

$$F_{q_0} = \begin{pmatrix} 0.990 & 0.041 \\ 0.009 & .958 \end{pmatrix}, \quad F_{q_1} = \begin{pmatrix} 0.962 & .041 \\ 0.037 & .958 \end{pmatrix}.$$

We then constructed corrected probability vector $\vec{P}_{CHzz\,c}$, from the experimentally obtained probability vector $\vec{P}_{CHzz} = \text{Tr}(\rho\ \text{CNOT}H\ \Pi_i H \otimes \Pi_j\ \text{CNOT})$. This results in the extraction of uncorrected experimental Bell states $|\Phi_\pm\rangle^{(\text{Expt})}$, $|\Psi_\pm\rangle^{(\text{Expt})}$ as well as the corrected ones $|\Phi_\pm\rangle^{(\text{Corr})}$, $|\Psi_\pm\rangle^{(\text{Corr})}$ (retrieved from error-mitigated probability vector $\vec{P}_{CHzz\,c}$) for all the four Bell states.

Quantum fidelity of theoretical and experimentally tomographed bell states before and after error-mitigation: Quantum fidelity (R. Jozsa, 1994) of any two density matrices ρ and σ given by

$$F(\rho,\sigma) = \text{Tr}\left(\rho^{1/2}\,\sigma\,\rho^{1/2}\right)^{1/2}$$

is a measure of how close are the two states. For pure states $\rho = |\psi\rangle\langle\psi|$ and $\sigma = |\phi\rangle\langle\phi|$ fidelity reduces to

$$F(|\psi\rangle,|\phi\rangle) = |\langle\psi|\phi\rangle|.$$

We have evaluated quantum fidelities (i) $F\left(|\Phi_\pm\rangle^{(\text{Expt})},||\Phi_\pm\rangle\right)$, $F\left(|\Psi_\pm\rangle^{(\text{Expt})},|\Psi_\pm\rangle\right)$ and (ii) $F\left(|\Phi_\pm\rangle^{(\text{Corr})},|\Phi_\pm\rangle\right)$, $F\left(|\Psi_\pm\rangle^{(\text{Corr})},|\Psi_\pm\rangle\right)$ of experimentally reconstructed Bell state density matrices before and after error mitigation.

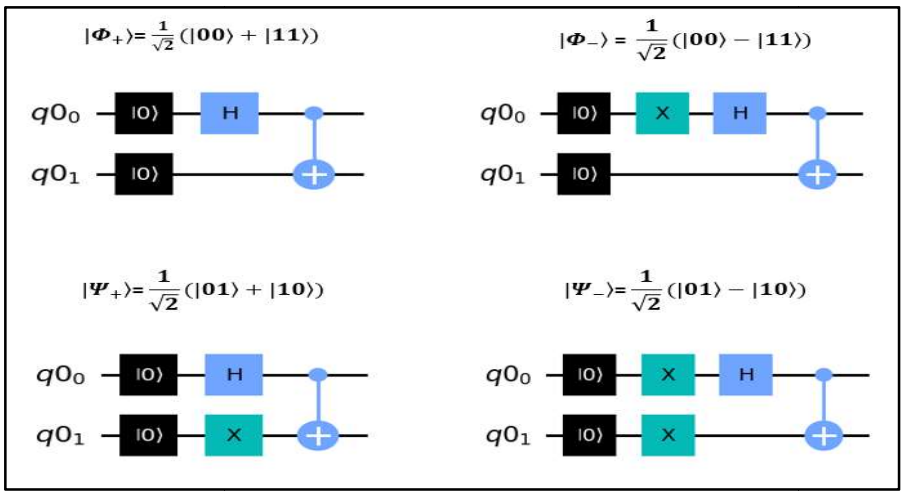

Figure 2. Quantum circuits employed for creating Bell states

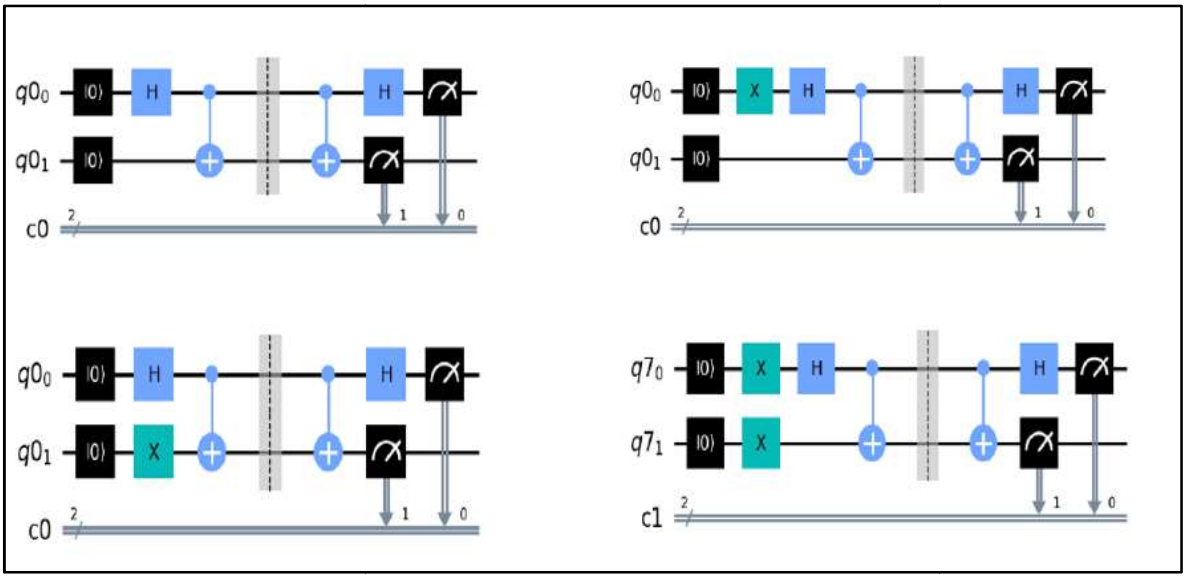

Figure 3. Quantum circuits for the tomographic operation ($H \otimes I$) CNOTfollowed by Z measurements

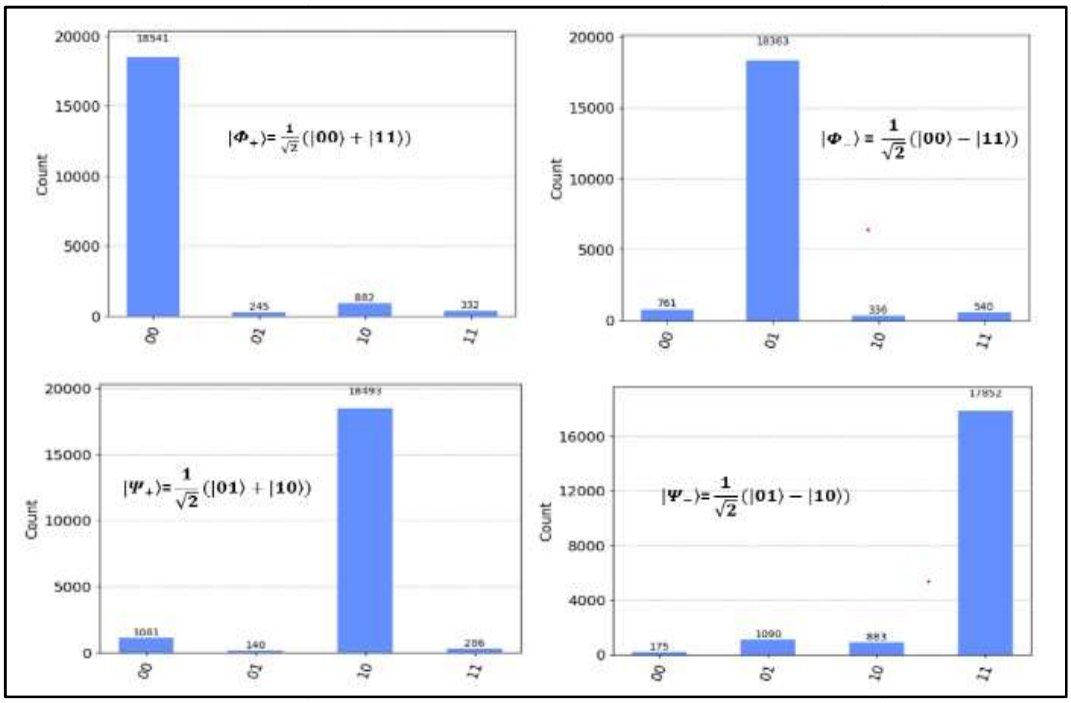

Figure 4. Counts recorded in one of the five experimental trials for all four Bell states. Total number of counts: 20,000.

Table 3. Quantum fidelities of Bell states before and after error-mitigation

Bell state $\|\Phi_+\rangle = \frac{\|00\rangle+\|11\rangle}{\sqrt{2}}$			**Bell state** $\|\Phi_-\rangle = \frac{\|00\rangle-\|11\rangle}{\sqrt{2}}$		
Trial No.	$F(\|\Phi_+\rangle^{(\text{Expt})}, \|\Phi_+\rangle)$	$F(\|\Phi_+\rangle^{(\text{Corr})}, \|\Phi_+\rangle)$	Trial No.	$F(\|\Phi_-\rangle^{(\text{Expt})}, \|\Phi_-\rangle)$	$F(\|\Phi_-\rangle^{(\text{Corr})}, \|\Phi_-\rangle)$
1	0.92	0.97		0.92	0.98
2	0.96	0.99		0.92	0.98
3	0.95	0.98		0.89	0.95
4	0.98	0.99		0.94	0.99
5	0.98	0.99		0.95	0.99
Bell state $\|\Psi_+\rangle = \frac{\|01\rangle+\|10\rangle}{\sqrt{2}}$			**Bell state** $\|\Psi_-\rangle = \frac{\|01\rangle-\|10\rangle}{\sqrt{2}}$		
Trial No.	$F(\|\Psi_+\rangle^{(\text{Expt})}, \|\Psi_+\rangle)$	$F(\|\Psi_+\rangle^{(\text{Corr})}, \|\Psi_+\rangle)$	Trial No	$F(\|\Psi_-\rangle^{(\text{Expt})}, \|\Psi_-\rangle)$	$F(\|\Psi_-\rangle^{(\text{Corr})}, \|\Psi_-\rangle)$
1	0.89	0.97		0.92	0.97
2	0.90	0.98		0.93	0.98
3	0.88	0.96		0.92	0.97
4	0.92	0.99		0.95	0.99
5	0.92	0.99		0.96	0.99

From Table 3 it is clearly seen that there is a marked improvement in quantum fidelity of the Bell states after error mitigation. We would like to point out that by employing the general two-qubit tomography scheme, as outlined in Table 2 using a set of 7 operations to reconstruct Bell states experimentally too highlights that error-mitigation results in improved quantum fidelity up to 0.97 in the case of Bell states (H. Talath *et al.,* 2023). However, Bell state tomography using $(H \otimes I)$ CNOToperation followed by z measurement on the qubits leads to better precision after error-mitigation is carried out.

SUMMARY

We have investigated the performance of IBM open access 7-qubit quantum processor *ibmq_nairobi* for Bell state tomography. By incorporating the operation $(H \otimes I)$ CNOT followed by z measurements on the zeroth and first qubits q0, q1 of *ibmq_nairobi* quantum processor we reconstruct the Bell states experimentally. We employ the standard measurement error-mitigation methodsa nd extract corrected experimental probability vectors associated with Bell state measurements. It is clearly established that the *quantum fidelity* evaluated after error-mitigation is better than that obtained before error-mitigation. Our results serve as a proof-of-principle demonstration of the basic tomography process using NISQ quantum processors.

Acknowledgements: ARU and Sudha are supported by Department of Science and Technology (DST), India, No. DST/ICPS/QUST/ 2018/107; ASH acknowledges funding from Foundation for Polish Science (IRAP Project, ICTQT, contract no. MAB/2018/5, co-financed by EU within Smart Growth Operational Programme).

REFERENCES

A. Barenco, C. H. Bennett, R. Cleve, D. P. DiVincenzo, N. Margolus, P. Shor, T. Sleator, J. A. Smolin, H. Weinfurter, (1993), Elementary gates for quantum computation,*Phys. Rev. A*Vol. 52, No. 5, pp.3457-3467

A. Montanaro, (2016), Quantum algorithms: An overview, *npj Quantum Inf.*Vol. 2, p.15023

A. W. R. Smith, K. E. Khosla, C. N. Self, M. S. Kim, (2021),Qubit readout error mitigation with bit-flip averaging,*Sci. Adv.*Vol. 7, No. 47, p. eabi8009 breaking with a superconducting quantum processor,*Comm. Phys*. Vol. 4**,** p.*26*

D. Qin, X. Xu, Y. Li, (2022),An overview of quantum error mitigation formulas*,* Chin. Phys. B Vol.31,

H. Talath, B. P. Govindaraja, B. G. Divyamani, H. S. Akshata, A. R. Usha Devi, Sudha, (2023),Tomography scheme for 2-qubit states using IBM 7-qubit open access quantum processor ibmq_nairobi*, Proceedings of 14th National Women's Science Congress*, (in print).

IBM quantum computing platform (2023) https://quantum-computing.ibm.com/

J. Preskill, (2018), Quantum Computing in the NISQ era and beyond, *Quantum,*Vol. 2, p.79 p.090306

R. Jozsa, (1994),Fidelity for Mixed Quantum States, *J. Mod. Opt*. Vol. 41, No. 12,pp. 2315-2323

S. Dogra, A. A. Melnikov, G. S. Paraoanu, (2021), Quantum simulation of parity–time symmetry

****